Microphase Separation Study of Amphiphilic ROMP Block Copolymers by SAXS and TEM

Kurt Stubenrauch,[†] Gerhard Fritz-Popovski,*[,‡] Elisabeth Ingolić,[§] Werner Grogger,[§] Otto Glatter,[‡] Franz Stelzer,[†] and Gregor Trimmel*[,†]

Institute for Chemistry and Technology of Organic Materials, Graz University of Technology, Stremayrgasse 16, 8010 Graz, Austria; Institute of Chemistry, University of Graz, Heinrichstrasse 28, 8010 Graz, Austria; and Research Institute for Electron Microscopy and Fine Structure Research, Steyrergasse 17, 8010 Graz, Austria

Received January 23, 2007; Revised Manuscript Received March 19, 2007

ABSTRACT: The self-assembly of block copolymers to form well-ordered structures is of great interest for the design of hierarchical materials. In this contribution, the morphologies and properties of well-defined block copolymers with narrow molecular weight distributions prepared by ring-opening metathesis polymerization are studied. Two series of amphiphilic AB-block copolymers poly[(*endo,exo*[2.2.1]bicyclohept-5-ene-2,3-dicarboxylic acid dimethyl ester)-*b*-(*endo,exo*[2.2.1]bicyclohept-5-ene-2,3-dicarboxylic acid)] of different block ratios and lengths were investigated by thermal analysis, small-angle X-ray scattering, and transmission electron microscopy. As observed by thermal gravimetric analysis and FTIR spectroscopy, the free carboxylic acid functionalities lead to anhydride formation at higher temperatures so that direct observation of the melt morphologies is not possible. However, by drop-casting polymer solutions in THF, which is a nonselective solvent for this type of block copolymer, well-ordered films were prepared. A variety of structured morphologies of block copolymers with different compositions was obtained. Perfectly ordered lamellar phases can be observed for AB-block copolymers where both blocks are of equal size. For block copolymers with ratios that deviate from 1:1, morphologies like lamellae with different lamella size, hexagonal cylinders, and globules with liquidlike packing were found.

Introduction

The creation of well-ordered nanostructures in materials is reliant on the design of well-defined chemical structures. The use of amphiphilic block copolymers is a promising approach to build such structured materials.[1,2] These block copolymers are composed of two or more immiscible blocks covalently bonded to each other, so that phase separation can only occur on the nanoscale, leading to morphologies with crystal-like order. A variety of ordered structures with different lengths can be obtained as a result of the self-assembly of block copolymers. The thermodynamic stable morphologies of AB-block copolymers are determined by the degree of polymerization N, the Flory−Huggins parameter χ, and the volume fractions of both blocks. If χ and the degree of polymerization are above a certain threshold, polymers of identical block length form lamellar structures. Changing the ratio of the two blocks results in a range of structures from bicontinuous cubic *Ia3d* structures through hexagonal and bcc spherical structures to close-packed spheres and disordered systems.[3−6]

From the synthetic point of view, obtaining highly ordered materials requires preparation and/or purification methods that produce block copolymers with a narrow distribution of molecular weights. Among several methods such as anionic polymerization,[7] atom transfer radical polymerization (ATRP),[8] reversible addition−fragmentation chain transfer radical polymerization (RAFT),[9] and others, ring-opening metathesis polymerization (ROMP)[10,11] fulfills these requirements very well. Several groups have demonstrated that this method is useful for obtaining polymers and block copolymers with low polydispersity indices.[12,13] The tolerance of recently developed ruthenium initiators[11,14] vs different functionalities and polarities exceeds that of most other polymerization techniques, and the living nature of ROMP makes it particularly valuable for the preparation of block copolymers with different functionalities. In addition, the potential for side- and end-functionalization of such polymers opens the way to new highly ordered functionalized materials. Several aspects of well-defined ROMP block copolymers have been investigated, such as their use as drug delivering material,[15] the formation of micelles and nanoparticles,[16−20] as polymers with special electrooptical and electroactive properties,[21,22] and for the preparation of inorganic nanoparticles and hybrid materials.[23−37] Especially for the preparation of inorganic hybrid materials self-assembled morphologies in the bulk have been studied. For pristine ROMP block copolymers, however, studies on the bulk morphologies are rare.[38]

Recently, we have shown that it is possible to tune the micelle size as well as the core and shell size of the micelles precisely via the composition of block copolymers prepared by ROMP.[18] For that study we synthesized two series of AB-block copolymers poly[(*endo,exo*[2.2.1]bicyclohept-5-ene-2,3-dicarboxylic acid dimethyl ester)-*b*-(*endo,exo*[2.2.1]bicyclohept-5-ene-2,3-dicarboxylic acid)]. For the first series the overall monomer/

* Corresponding authors. Gregor Trimmel: e-mail gregor.trimmel@tugraz.at, Tel ++43316-8734958, Fax ++43316-8738951. Gerhard Fritz-Popovski: e-mail gerhard.fritz@uni-graz.at, Tel ++43316-3805415, Fax ++43316-3809850.

[†] Graz University of Technology.

[‡] University of Graz.

[§] Research Institute for Electron Microscopy and Fine Structure Research.

10.1021/ma070181q CCC: $37.00
Published on Web 05/27/2007

catalyst ratio was kept the same (200:1), but the ratio of lyophilic monomer to lyophobic monomer was altered. For the second series the lyophilic to lyophobic ratio was kept the same, namely 1:1, but the overall monomer/catalyst ratio was varied.

In the present work we investigate the properties and the microphase separation of these polymers in bulk phase. Because of the low thermal stability of the acidic block, the sample preparation was only possible from solution. Although it is hardly possible to get equilibrium phases, we will show that well-ordered morphologies can be obtained by this method. As several block copolymers with different ratios and lengths are available for the investigation with small-angle X-ray scattering (SAXS) and transmission electron microscopy (TEM), it is expected that different ordered morphologies can be observed. SAXS is a particularly powerful tool for obtaining integral information about the structure in the bulk.[39]

Experiment and Theory

The synthesis of both the monomers and the polymers has been reported elsewhere.[18]

Gel permeation chromatography (GPC): the weight and number average of the molecular weights (M_w and M_n) and the polydispersity index (PDI) were determined by gel permeation chromatography with THF as the solvent using the following arrangement. Merck Hitachi L6000 pump, separation columns from the Polymer Standard Service, 8 × 300 mm STV 5 μm grade size (10^6, 10^4, and 10^3 Å), combined refractive index−viscosity detector from Viscotec, Viscotec 200. Polystyrene standards purchased from the Polymer Standard Service were used for calibration.

^{1}H NMR and ^{13}C NMR spectra were recorded on a Varian INOVA 500 MHz spectrometer operating at 500 and 125 MHz, respectively, and were referenced to $SiMe_4$. A relaxation delay of 10 s and 45° pulse were used for acquisition of the ^{1}H NMR spectra to guarantee accurate integration of the corresponding signals. The solvent residual peaks of $CDCl_3$ and DMSO-d_6 were used for referencing the spectra to 7.26, 77.16 ppm and 2.50, 39.52 ppm, respectively.[40]

Differential scanning calorimetry (DSC) measurements were carried out on a Perkin-Elmer Pyris Diamond under a nitrogen flow of 20 mL/min and a heating rate of 10 °C/min. Glass transition temperatures (T_g) were taken from the second heating run and were read as the midpoint of change in heat capacity.

Combined DSC/thermogravimetric analysis (TGA) measurements were performed with a Polymer Laboratories simultaneous thermal analyzer (STA 625) under nitrogen flow of 35 mL/min and a heating rate of 10 °C/min (crucibles: aluminum from Rheometric Scientific).

FT-IR spectra were recorded with a Perkin-Elmer Spectrum One instrument (spectral range between 4000 and 450 cm^{-1}). All FT-IR spectra of the samples were recorded in transmission mode (films on CaF_2 discs or silicon wafers).

Transmission electron microscopy (TEM) images were acquired on a Tecnai G^2 12 (FEI Co.) equipped with a CCD camera (Gatan Bioscan) at 100 kV. Samples were placed in gelatin capsules containing Epofix (Struers). The capsules were placed in an exsiccator overnight—the polymerization takes place at room temperature. The capsules with the samples were trimmed to a pyramid. Ruthenium tetroxide and osmium tetroxide were used to harden and to stain the samples for contrast enhancement. Using a diamond knife (Diatome), 75−85 nm ultrathin sections were cut on a Leica Ultracut E ultramicrotome and collected onto 100 mesh copper grids with a support film of Pioloform.

Dynamic light scattering (DLS): For the DLS measurements we used a laboratory built goniometer, which was equipped with single mode fiber optics and an ALV single photon detector. The light source was a Verdi V5 diode laser from Coherent with a wavelength of 532 nm and a maximum output power of 5 W (typically laser power used 0.5 W). The data acquisition was performed with an ALV 5000 multiple τ digital correlator. This allows a minimum time interval of 12.5 ns for the correlation function. The ALV-5000/E software package was used to record and store the correlation functions. All experiments were carried out at 25 °C and at a scattering angle of 90°. Each sample was measured 10 times for 60 s. The obtained correlation functions were averaged and used for calculation of the size distributions. We used the ORT software to determine the intensity weighted size distribution functions.[41]

The SAXS equipment was a SAXSess camera (Anton-Paar, Graz, Austria) using an X-ray generator (Philips, PW 1730/10) operated at 40 kV and 50 mA with a sealed-tube Cu anode. A Göbel mirror was used to convert the divergent polychromatic X-ray beam into a collimated line-shaped beam of Cu Kα radiation ($\lambda = 0.154$ nm). The 2D scattering pattern was recorded by an imaging-plate detector (model Fuji BAS1800 from Raytest, Straubenhardt, Germany) and integrated into the one-dimensional scattering function $I(q)$ using SAXSQuant software (Anton-Paar). The samples were measured at room temperature.

Polymer films for SAXS experiments were drop-casted from 10 wt % THF solutions on silicon substrates. After drying under ambient atmosphere, the films were removed from the substrate. A specimen holder was designed so that the freestanding polymer films were irradiated under the same defined angle (24°).

General Relations from SAXS. The scattering intensity at large scattering angles corresponds to a q^{-4} behavior[42]

$$I(q) \rightarrow (\Delta\rho)^2 \frac{2\pi}{q^4} S \tag{1}$$

where the absolute value of the scattering vector q is related to the wavelength λ and the scattering angle θ by $q = (4\pi/\lambda)\sin(\theta/2)$. The scattering length difference to the average scattering length is $\Delta\rho$, and the surface area of the structures is S. Experimentally, it is however difficult to obtain the absolute intensities required to compute S. Therefore, this expression is related to the invariant Q

$$Q \equiv \int_0^\infty q^2 I(q)\, \mathrm{d}q = V(\Delta\rho)^2 \varphi(1-\varphi) 2\pi^2 \tag{2}$$

where V is the volume of the structures and φ is the volume fraction of one of the two components. If eqs 1 and 2 are combined

$$\frac{\lim_{q\to\infty} q^4 I(q)}{\int_0^\infty q^2 I(q)\, \mathrm{d}q} = \frac{1}{\pi\varphi(1-\varphi)} \frac{S}{V} \tag{3}$$

is obtained, which allows the computation of the surface to volume ratio if the volume fraction of one component within the sample is known. The contrast term is canceled out in this ratio, and therefore absolute intensities are not necessary for this calculation. Instrumental broadening effects which appear in cameras using slit collimation and lead to measurement of a smeared intensity $\tilde{I}(q)$ instead of $I(q)$ change the equation to

$$\frac{\lim_{q\to\infty} q^3 \tilde{I}(q)}{\int_0^\infty q \tilde{I}(q)\, \mathrm{d}q} = \frac{1}{4\varphi(1-\varphi)} \frac{S}{V} \tag{4}$$

Characterization of Lamellar Structures. The evaluation of scattering curves of lamellar structures is, according to Vonk,[43] best done if based on the Patterson function. This function is better known within the field of small-angle X-ray scattering as correlation function $\gamma_0(r)$.[42] As a simple Fourier transform of the scattering curve, the correlation function contains the same information as the scattering curve in reciprocal space. This information in $\gamma_0(r)$ is, however, in real space and therefore easier to interpret.

The scattering intensity of a lamellar stack can be separated into two components: one that arises from the theoretically infinite

extension of the lamellae in two dimensions and the other that results from a one-dimensional contribution $I_1(q)$ due to electron density fluctuations normal to the surface of the lamellae

$$I_1(q) = \frac{q^2 I(q)}{2\pi A} \tag{5}$$

where $I(q)$ is the scattering intensity and A the surface area of one lamella. $I_1(q)$ can be related to the one-dimensional correlation function $\gamma_1(r)$ by the Fourier transformation:[44]

$$\gamma_1(r) = \frac{1}{\pi}\int_0^\infty I_1(q)\cos(qr)\,\mathrm{d}q \tag{6}$$

The correlation function may be obtained by indirect Fourier transformation[45] or by direct transformation techniques. In the case of a camera using slit geometry the necessary transformation is

$$\gamma_1(r) = \frac{\int_0^\infty q\tilde{I}(q)[J_0(qr) - (qr)J_1(qr)]\,\mathrm{d}q}{\int_0^\infty q\tilde{I}(q)\,\mathrm{d}q} \tag{7}$$

where J_0 and J_1 are zero- and first-order Bessel functions.

The resulting one-dimensional correlation functions can be interpreted directly or models can be approximated in order to obtain numbers that can be used to compare the samples more easily. The model used approximated the width of the two blocks within the lamellar stacks. It is unlikely that a perfect crystal lattice will be formed. Therefore, Reinhold distribution functions[46] were taken into account in order to describe the deviations statistically:

$$P(x) = \begin{cases} 0 & x \le \bar{x}(1-2\gamma) \\ \dfrac{x-\bar{x}(1-2\gamma)}{(\gamma\bar{x})^2}\exp\left(-\dfrac{x-\bar{x}(1-2\gamma)}{\gamma\bar{x}}\right) & x > \bar{x}(1-2\gamma) \end{cases} \tag{8}$$

The distribution width parameter γ was limited in the range 0−0.5, and it is related to the mean deviation σ by $\sigma = (\gamma\bar{x})\sqrt{2}$.

Generalized Indirect Fourier Transformation. The indirect Fourier transformation is a tool for the largely model free evaluation of scattering data. It is based on a linear combination of basis functions that represents the pair distance distribution function $p(r)$,[47,48] which is the real-space analogue of the scattering intensity

$$I(q) = 4\pi\int_0^\infty p(r)\frac{\sin(qr)}{qr}\,\mathrm{d}r \tag{9}$$

The main advantage of this transformation is that $p(r)$ contains the same information as $I(q)$, but in real space. This allows for direct interpretation of the data and makes the design of models for the structures observed much simpler.[49]

In the case of higher concentrations, where interaction effects between the structures cannot be neglected, it is necessary to use the modified generalized indirect Fourier transformation technique.[50,51] This method separates the scattering intensities into contributions due to individual structures and contributions due to the arrangement of the structures based on models for the interaction.[52] An averaged effective hard-sphere model[53] that is based on the analytical Percus−Yevick solution[54] of the Ornstein−Zernicke equation[55] was used. A short introduction including references is given in the Supporting Information.

Results and Discussion

Amphiphilic block copolymers were prepared by ROMP. As the lyophobic monomer we chose *endo,exo*[2.2.1]bicyclohept-5-ene-2,3-dicarboxylic acid dimethyl ester and e*ndo,exo*[2.2.1]-bicyclohept-5-ene-2,3-dicarboxylic acid as the lyophilic part. The "first generation Grubbs" initiator $RuCl_2(PCy_3)_2(CHPh)$ (Cy = cyclohexyl) was used as the catalyst. We showed that by protection of the acidic groups as *tert*-butyl esters well-defined precursor block copolymers can be synthesized.[18] All the polymers prepared have low polydispersity indices determined by GPC and defined block sizes investigated by NMR spectroscopy.

Scheme 1. Transformation of the Precursor Block Copolymer into an Amphiphilic Block Copolymer

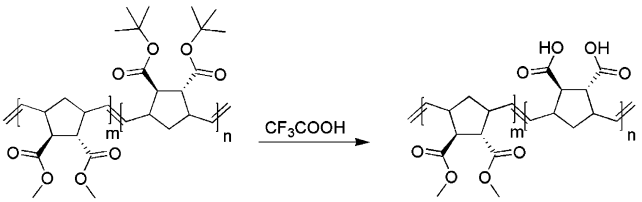

Three block copolymers **1**−**3** with equal block size but different overall length were prepared to investigate the influence of the degree of polymerization on the domain size of the self-assembled morphologies. Furthermore, block copolymers **5**−**10** with different block ratios but the same overall block copolymer length were synthesized to obtain different self-assembled morphologies in the solid state. The block sizes and the block ratios of the different polymers are shown in Table 1. Homopolymers **4** and **11** were synthesized to complete the series.

The molecular weight distributions and the polydispersity indices of the precursor diblock copolymers were determined using GPC (Table 1). The GPC measurements were calibrated against polystyrene standards; nevertheless, the determined masses are in good agreement with the theoretical ones. By end-group analysis of the NMR spectra of polymer **1** and shorter oligomers, we have shown that the obtained GPC values are close to the real values of M_n.[18] On the basis of this, we estimated that deviations from the absolute values are below 15%.

After complete characterization of the block copolymers the *tert*-butyl groups were cleaved with trifluoroacetic acid, the precursor polymers were thus transformed into amphiphilic block copolymers, as depicted in Scheme 1. The physicochemial data of the polymers are listed in Table 1.

The glass transition temperatures of both the homopolymers **4** (82.4 °C) and **11** (83.4 °C) are almost identical, and consequently all T_gs of the precursor block copolymers are approximately equal.

Determination of the T_g after the transformation of the precursor block copolymer into the amphiphilic block copolymer was not possible because anhydride formation of the acid groups began at about 100 °C. Figure 1 shows the results of the thermogravimetric analysis of the homopolymer **4** which contains only dimethyl ester units in comparison to block copolymer **7** in the precursor state and after deprotection. Polymer **4** is stable to a very high temperature and only starts to degrade at 375 °C. The precursor block copolymer **7** (M_{125}:N_{75}) is stable up to 240 °C, and then the *tert*-butyl group is cleaved thermally. The weight loss of about 18% is in good agreement with the theoretical values for complete deprotection and loss of isobutene. However, the deprotected amphiphilic polymer **7** already shows a significant weight loss at temperatures from 100 to about 150 °C, which can be assigned to the loss of absorbed water and of water due to anhydride formation.

The formation of anhydrides was confirmed by FTIR spectroscopy. A film of amphiphilic block copolymer **7** was prepared on a silicon substrate and was heated to 100, 200, and 300 °C under inert atmosphere for 10 min in each case, and after every temperature step an IR spectrum was recorded. In Figure 2 the carbonyl peak area of the IR spectra is shown. In all four spectra one can clearly see a peak at 1732 cm^{-1} which

Table 1. Physicochemical Characteristics of the Amphiphilic Block Copolymers

sample no.	M^a	N^b	X_m NMR^c	$M_{calc}{}^d$ (g/mol)	M_n (GPC)^e (g/mol)	$M_{n\ dep,calc}{}^f$ (g/mol)	PDI^g	$T_g{}^h$ (°C)
1	40	40	1.0	20 384	24 900	15 800	1.08	n.d.
2	75	75	0.90	37 544	35 900	27 900	1.16	81.9
3	100	100	1.0	49 737	54 100	42 100	1.13	83.4
4	200	0		41 637	47 100		1.13	82.4
5	175	25	7.2	44 317	44 900	41 700	1.15	82.5
6	150	50	3.2	46 408	49 300	43 600	1.15	80.3
7	125	75	1.7	48 562	53 600	44 400	1.14	83.2
8	75	125	0.62	52 699	51 200	35 800	1.11	83.8
9	50	150	0.31	54 774	54 900	37 800	1.07	83.7
10	25	175	0.14	56 878	54 000	35 400	1.07	83.5
11	0	200		58 982	54 700		1.05	83.4

[a] Theoretical number of lyophobic units (*endo*,*exo*[2.2.1]bicyclohept-5-ene-2,3-dicarboxylic acid dimethyl ester). [b] Theoretical number of lyophilic units (*endo*,*exo*[2.2.1]bicyclohept-5-ene-2,3-dicarboxylic acid). [c] Ratio of lyophobic block/lyophilic block determined via integration of the ^{1}H NMR spectra (relaxation time 10 s). [d] Calculated molecular weight of the precursor block copolymer. [e] Number-average of the molecular weight distribution of the precursor block copolymers determined by GPC. [f] Calculated molecular weight of the amphiphilic block copolymers based on GPC and NMR data. [g] Polydispersity index of the precursor block copolymers determined by GPC. [h] Glass transition temperature of the precursor block copolymers determined by DSC.

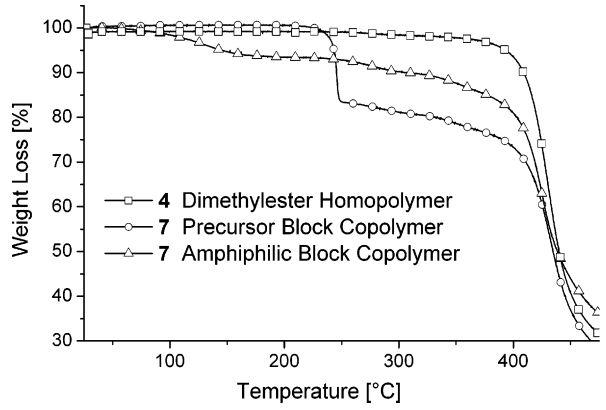

Figure 1. Thermogravimetric analysis curves of homopolymer **4**, precursor block copolymer **7** (M_{125}:N_{75}), and amphiphilic block copolymer **7** (M_{125}:N_{75}).

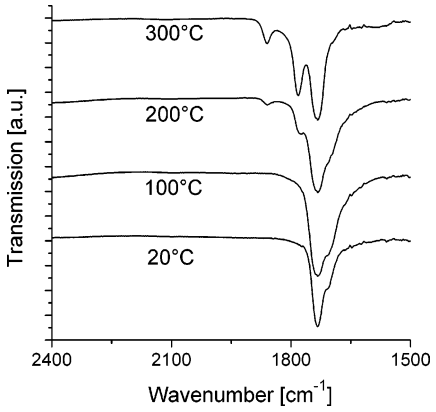

Figure 2. FT-IR spectra of amphiphilic block copolymer **7** (M_{125}:N_{75}) after treatment at different temperatures. The new peaks at 1783 and 1861 cm^{-1} can be assigned to anhydride formation.

can be assigned to the dimethyl ester. This peak has a shoulder at 1706 cm^{-1} which disappears with rising temperature and can be assigned to the carboxylic acid. In contrast, two carboxylic acid anhydride bands emerge at high temperatures at 1783 and 1861 cm^{-1} in the two spectra. The band at lower frequency is stronger than that one at higher frequency, which leads to the assumption that cyclic anhydrides are formed.[56]

Because of the anhydride formation, a thermal annealing step above the T_g of the two blocks is not possible. This low thermal stability of the block copolymers does not allow the direct investigations of melt morphologies and order−disorder transition by heating. This also inhibits experimental determination

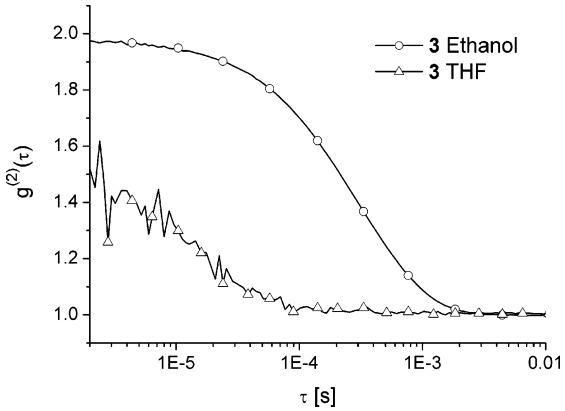

Figure 3. DLS correlation functions of block copolymer **3** (M_{100}:N_{100}) in ethanol and THF.

of the interaction parameter χ by SAXS as proposed by Leibler.[57]

As an alternative to thermal equilibration we used the film preparation through drying from a nonselective solvent. However, the achievement of true melt equilibrium often remains questionable, as truly nonselective solvents are rarely found—thus the obtained morphologies are strongly dependent on the used solvent—and the experimental parameters (partial pressure of solvent, rate of evaporation) are difficult to control.[58] In addition, the drying process can cause internal strain fields that influence the formation of morphologies. However, THF seems to be a nonselective solvent for the block copolymers studied in this work. In Figure 3, the DLS correlation functions of solutions of block copolymer **3** (M_{100}:N_{100}) in ethanol and THF are shown. It is clear that micelles (radius of about 21 nm) are only formed in ethanol, which is a selective solvent for the acidic block, whereas THF dissolves both blocks so that no aggregates are built. THF was therefore chosen as the solvent for the preparation of the block copolymer films. Polymer films were drop-casted from 10 wt % THF solutions onto silicon substrates. After slow drying under ambient atmosphere, we obtained optical clear or slightly yellowish films that were mechanically quite robust. The thicknesses of the films were about 30 μm. The films were removed from the substrate and investigated with SAXS and TEM.

For SAXS measurements, a special specimen holder was designed so that the polymer films were always irradiated under the same defined angle (24°) in order to increase the effective sample thickness. The scattering curves of all samples show correlation peaks (Figures 4 and 7) which demonstrate that interstructural ordering is an important feature within the studied

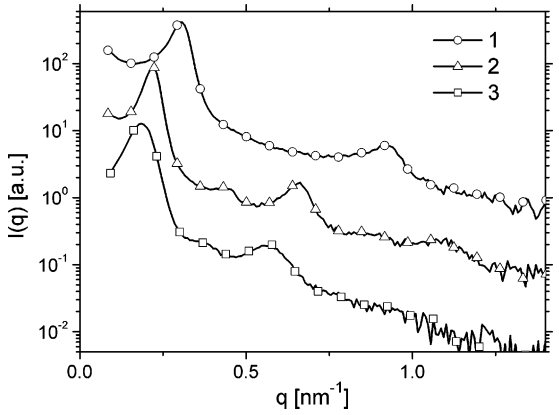

Figure 4. Scattering curves of block copolymer films with equal block size but different molecular weights. Every 10th point is marked. **1** (M_{40}:N_{40}), **2** (M_{75}:N_{75}), **3** (M_{100}:N_{100}).

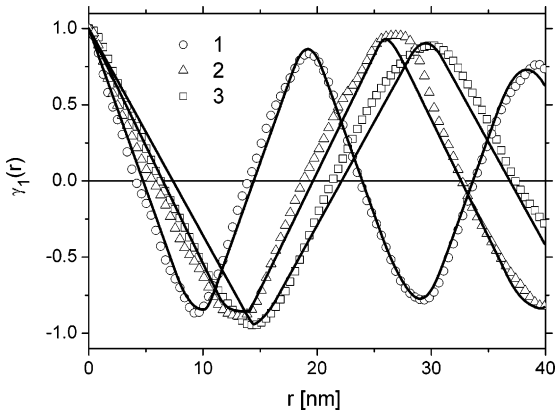

Figure 5. One-dimensional correlation functions of the block copolymer systems shown in Figure 4. The lines are the model approximations. **1** (M_{40}:N_{40}), **2** (M_{75}:N_{75}), **3** (M_{100}:N_{100}).

films. The films prepared from polymers with an identical number of monomers (polymers **1**−**3**) within the two blocks have equidistant peaks. The first- and third-order peaks are clearly visible while second- and higher-order ones are weak. This is a typical sign of lamellar structures where the alternating blocks within the lamellar stacks are of identical thickness.

This behavior allows the use of the approach of Vonk and Kortleve[43] for the evaluation of the data. Transformation of the scattering curve into the $\gamma_1(r)$ function results in curves of sawtooth shape (Figure 5). The lack of a flat part at the minima and the fact that all these curves reach minima that are close to −1 indicate that the two blocks are of approximately equal length. This is due to the fact that the depth of the minimum is $-\varphi/(1-\varphi)$, where φ is the volume fraction of the minority block. Additionally, the first maxima at $r > 0$ are also close to 1, which proves that the order within the stack is high, since otherwise it should be damped due to imperfect correlations between the layers. Finally, these maxima move to higher r values with increasing lengths of the blocks, which is expected, since they correspond to the repeat distance within the stack.

The model described in the experimental section was approximated to these $\gamma_1(r)$ functions in order to quantify the observations made above. The results of these approximations are listed in Table 2. It is found that the lengths of the two blocks are identical to within 21% and that within this series the agreement is better for polymers with higher molecular weight. The repeat distance increases with lengths of the chains from 18.6 nm (polymer **1**) to 28.8 nm (polymer **3**). The standard deviations of both block lengths are small (≤0.6 nm), which

Table 2. Results from Model Approximations to $\gamma_1(r)$

sample	ratio	width 1 (nm)	width 2 (nm)	std dev width 1 (nm)	std dev width 2 (nm)
1	M_{40}:N_{40}	10.43	8.21	0.30	0.42
2	M_{75}:N_{75}	12.08	14.03	0.63	0.02
3	M_{100}:N_{100}	14.43	14.41	0.10	0.49
7	M_{125}:N_{75}	11.78	21.19	0.02	1.59

Table 3. Surface-to-Volume Ratio of Structures within Polymer Films

sample	ratio	surface/volume (nm^{-1})
1	M_{40}:N_{40}	0.131 ± 0.005
2	M_{75}:N_{75}	0.086 ± 0.005
3	M_{100}:N_{100}	0.060 ± 0.003
5	M_{175}:N_{25}	0.161 ± 0.006
6	M_{150}:N_{50}	0.068 ± 0.003
7	M_{125}:N_{75}	0.181 ± 0.019
8	M_{75}:$N1_{25}$	0.187 ± 0.006
9	M_{50}:N_{150}	0.068 ± 0.003
10	M_{25}:N_{175}	0.112 ± 0.006

leads to the high degree of order and the weak damping of the oscillations observed for the $\gamma_1(r)$ functions. The repeating distances scale with polymer length to a power of 0.49 ± 0.05, indicating that the samples investigated are within the weak segregation limit, where a scaling with $N^{0.5}$ is expected.[5]

The findings from the model agree with the results of the surface to volume calculations (Table 3). These values are close to the theoretical value $2/d$ for lamellar stacks, where d is the repeat distance within the stack. Therefore, the lamellae cannot be undulating strongly and they cannot show high surface roughness or many holes, since all these features would increase the surface-to-volume ratio.

Transmission electron microscopy (TEM) confirms the results obtained by SAXS. TEM pictures of block copolymers **1** and **3** are depicted in Figure 6. One can clearly see a well-ordered lamellar morphology for both polymers. The repeating unit distances for the double layers seen in the TEM pictures (17.5 nm for polymer **1**, 30 nm for polymer **3**) are in good agreement with the values from the SAXS measurements. In both cases the dark and bright lamellae are of similar size. These results indicate that the volume fractions of the hydrophilic and hydrophobic blocks are comparable.

Scattering curves of samples where the total polymer length is kept constant, but where the monomer ratio of the two blocks is varied, still show interaction peaks due to the structures formed (Figure 7). The degree of order decreases the more the ratio of the two block sizes deviates from unity, which can be seen by the decrease of higher-order interaction peaks.

In the case of block copolymer **7** (M_{125}:N_{75}) where the ratio of the two blocks is still close to one, lamellar order is preserved, which can be seen from the equidistant interaction peaks. It is therefore still possible to apply the approach of Vonk and Kortleve to evaluate the data. Figure 8 shows the one-dimensional correlation functions $\gamma_1(r)$ of the lamellar structures in comparison to polymer **3** (M_{100}:N_{100}). The most distinct feature of the curve of polymer **7** is the change from a sawtooth shape to a flat part in the minimum. This indicates that the two blocks are no longer of identical size. The ratio of the volume occupied by the two blocks can be estimated from the depth of the minima for **7** to be 1.8:1. This value was confirmed by a model approximation to the function which is in good agreement with the expected 1.7:1 ratio of the chemical composition. This model also reveals that **7** has a considerably higher standard deviation for the lengths of the blocks than the 1:1 samples, which is reflected in their less precise ordering (see Table 2). The surface-to-volume ratio of 0.0181 also shows

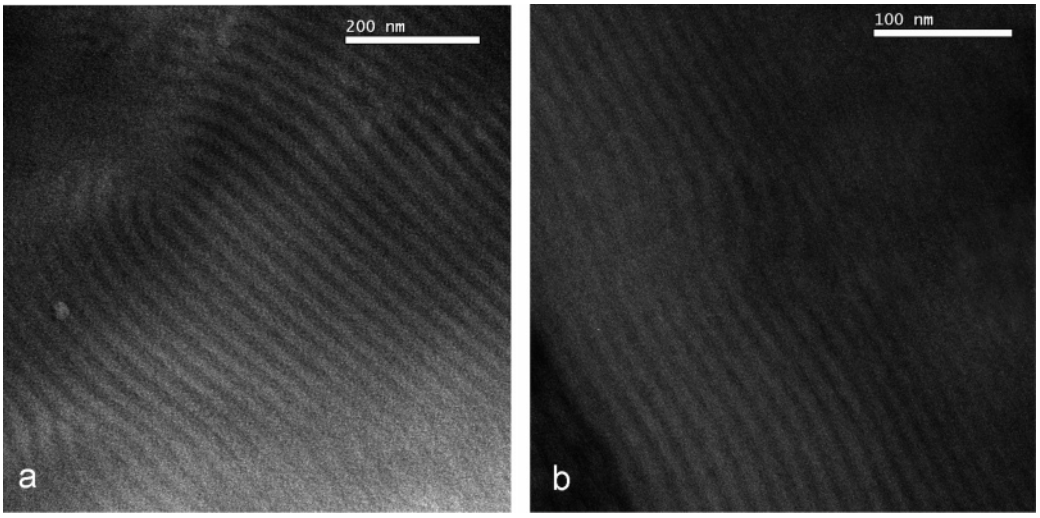

Figure 6. TEM pictures of (a) polymer **3** (M_{100}:N_{100}) and (b) polymer **1** (M_{40}:N_{40}).

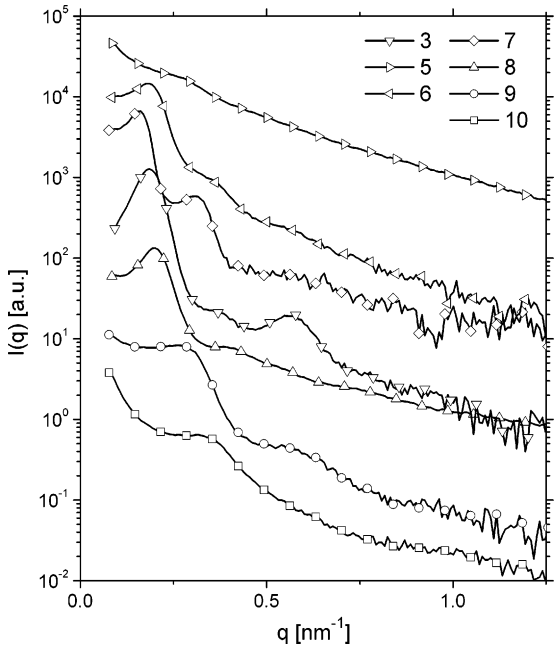

Figure 7. Scattering curves of block copolymer films with different block ratios. Curves have been shifted vertically for better visibility. Every 10th point is marked. **3** (M_{100}:N_{100}), **5** (M_{175}:N_{25}), **6** (M_{150}:N_{50}), **7** (M_{125}:N_{75}), **8** (M_{75}:N_{125}), **9** (M_{50}:N_{150}), **10** (M_{25}:N_{175}).

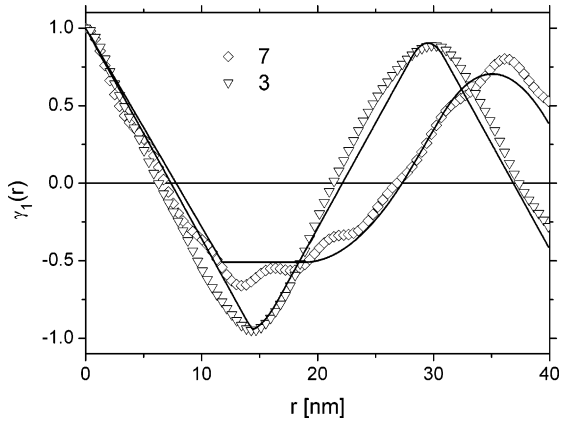

Figure 8. Comparison of the one-dimensional correlation functions of the block copolymer **3** (M_{100}:N_{100}) and **7** (M_{125}:N_{75}). The lines are the model approximations.

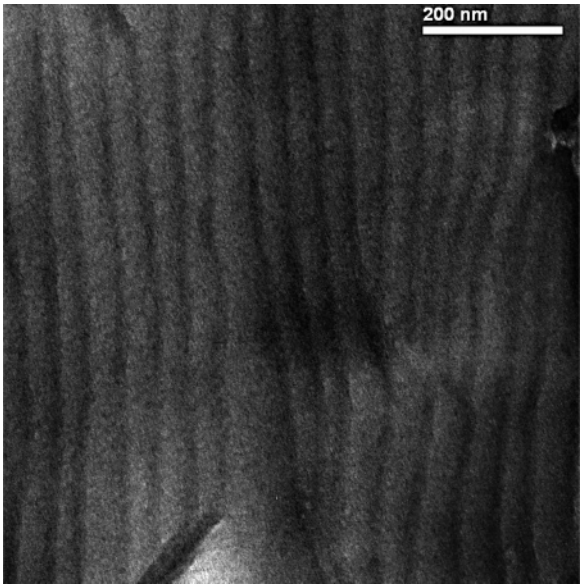

Figure 9. TEM image of block copolymer **7** (M_{125}:N_{75}).

a considerable increase of 3 times the ratio expected for a perfect lamellar stack, which proves that the lamellae formed by these polymers show roughness, although it is not clear from this single value which kind of deviation from perfectly flat structures might be the cause. The TEM picture of block copolymer **7** (Figure 9) sustains this structure.

The SAXS pattern of polymer **8** (M_{75}:N_{125}) shows one strong correlation peak at $q^* = 0.20$ nm^{-1} and a weak and broad peak at about 0.38 nm^{-1}. This latter value corresponds to $1.9q^*$ and lies between the theoretical values of a hexagonal peak $1.73q^*$ and the second-order peak $2q^*$ that would also be present in a lamellar phase. These findings indicate a hexagonal structure, where the two peaks cannot be resolved. However, a similar value (1.88) was found for the hexagonal perforated layer phase.[59] The phase cannot be determined unambiguously by SAXS. TEM investigations (Figure 10) reveal that the block copolymer film consists of a hexagonal packed cylindrical phase (Figure 10a) with regions with quite unordered wormlike structures (Figure 10b). Combining the SAXS and TEM results, one can attribute the structure to a weakly ordered hexagonal phase. This low order also leads to an increase of the S/V value from the expected 0.064 nm^{-1} for perfect hexagonally ordered cylinders to 0.187 nm^{-1}.

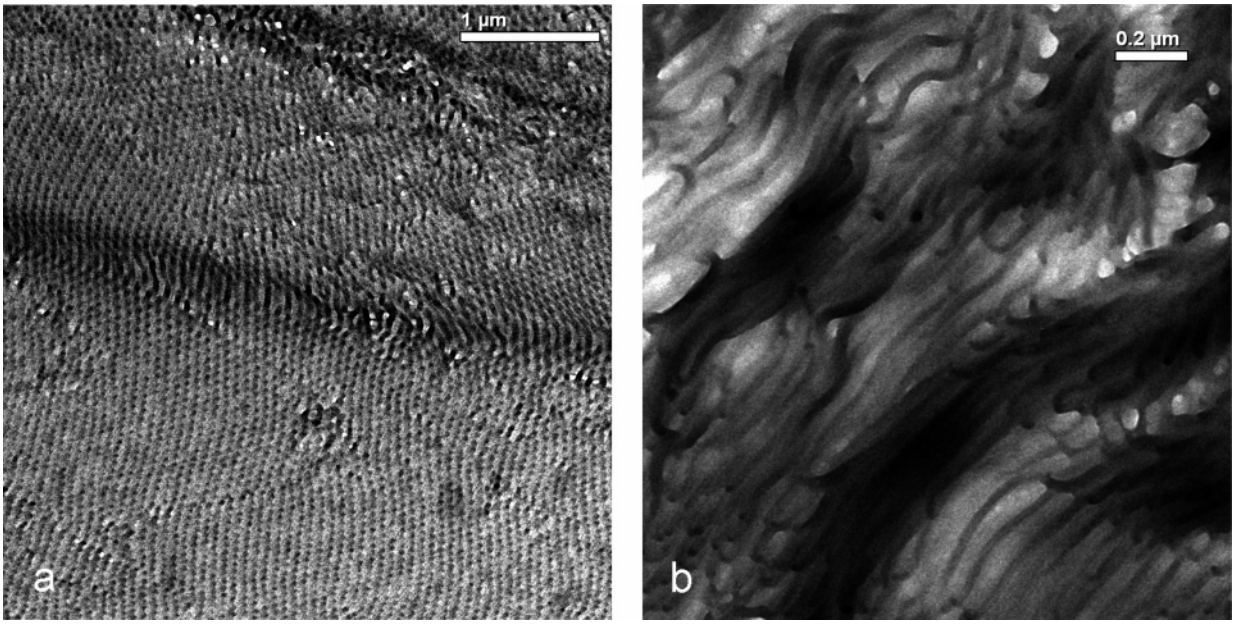

Figure 10. TEM pictures of polymer **8** (M_{75}:N_{125}): hexagonal cylindrical phase (a) and wormlike cylinders (b).

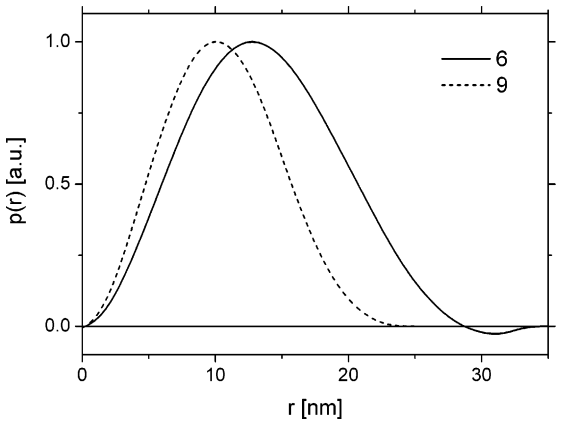

Figure 11. Pair distance distribution functions of polymers with block sizes **6** (M_{150}:N_{50}) and **9** (M_{50}:N_{150}).

The SAXS patterns of polymers **6** and **9** with ratios of M_{150}:N_{50} and M_{50}:N_{150} are best described by assuming globules with liquidlike packing.[60] The generalized indirect Fourier transformation results in $p(r)$ functions that are typical for globular objects, with a maximum dimension of 28 nm for **6** and of about 22 nm for **9** (Figure 11). Neither curve is completely symmetrical, which can be explained by either a size distribution or a deviation from perfect spherical shape.[61] It should be noted that deviations from spherical symmetry are hard to quantify for systems that show such strong interactions as these samples.[62] In any case, the parameters needed to describe the interaction effects result in interaction radii of 16.9 nm for **6** and 10.1 nm for **9**. These values are within the expected range, but they can be only a rough estimate because of the polydispersity or deviation from perfectly spherical shape in combination with high volume fractions. The effective volume fractions are 0.50 and 0.40. These values are definitely not close to the volume fractions of one of the two blocks, which are expected to be approximately 0.25 and 0.75 according to the chemical composition. Nevertheless, because of the covalent bonding of the blocks, the globules and the continuous component cannot arrange independently, leading to an effective volume fraction that depends on both blocks.

For both polymers the same rather low S/V ratio (0.068) was obtained. A crude estimation based on the position of the interaction peaks shows that the S/V ratios can be explained in terms of spheres with radii of about 15 and 9 nm, which is in reasonable agreement with the results obtained from the generalized indirect Fourier transformation.

Spherical structures in liquidlike arrangements were also observed when recording TEM pictures from the prepared films. TEM pictures of the block copolymers **6** and **9** are shown in Figure 12.

Polymers **5** (M_{175}:N_{25}) and **10** (M_{25}:N_{175}) still contain structures, but they are no longer well-ordered. The SAXS pattern cannot be explained by a liquidlike structure with spherical objects as for polymers **6** and **9**. Nevertheless the S/V ratios of 0.161 and 0.112, respectively, make it clear that these structures are also rather small or rough leading to such high values of this parameter. The low q-parts of the scattering curves show a pronounced increase of scattering intensity, which corresponds to long-range order that cannot be resolved in the SAXS experiments. This is in agreement with the TEM pictures (Figure 13), where the arrangement of the structures is clearly preferential within elongated aggregates. It is, however, important to note that the increase at low q is much stronger than the q^{-1} expected for linear aggregates, indicating a higher dimensionality of the structures. The correct value of the dimension cannot be pinpointed from the short q range available. The TEM pictures of polymer **5** and **10** are presented in Figure 13. Polymer **5** (175:25) shows spots of well-separated dark areas with dimension of approximately 4−10 nm. The TEM image of polymer **10** shows connected globular structures of about 20 nm. However, the preparation of this sample was difficult, and it seems that part of the polymer films dissolved during the cutting procedure in water.

Conclusion

In this contribution we investigated the bulk morphologies of amphiphilic diblock copolymers with narrow molecular weight distributions prepared by ROMP. Block copolymers of type poly[(*endo*,*exo*[2.2.1]bicyclohept-5-ene-2,3-dicarboxylic acid dimethyl ester)-*b*-(*endo*,*exo*[2.2.1]bicyclohept-5-ene-2,3-dicarboxylic acid)] were used for the morphology studies. The

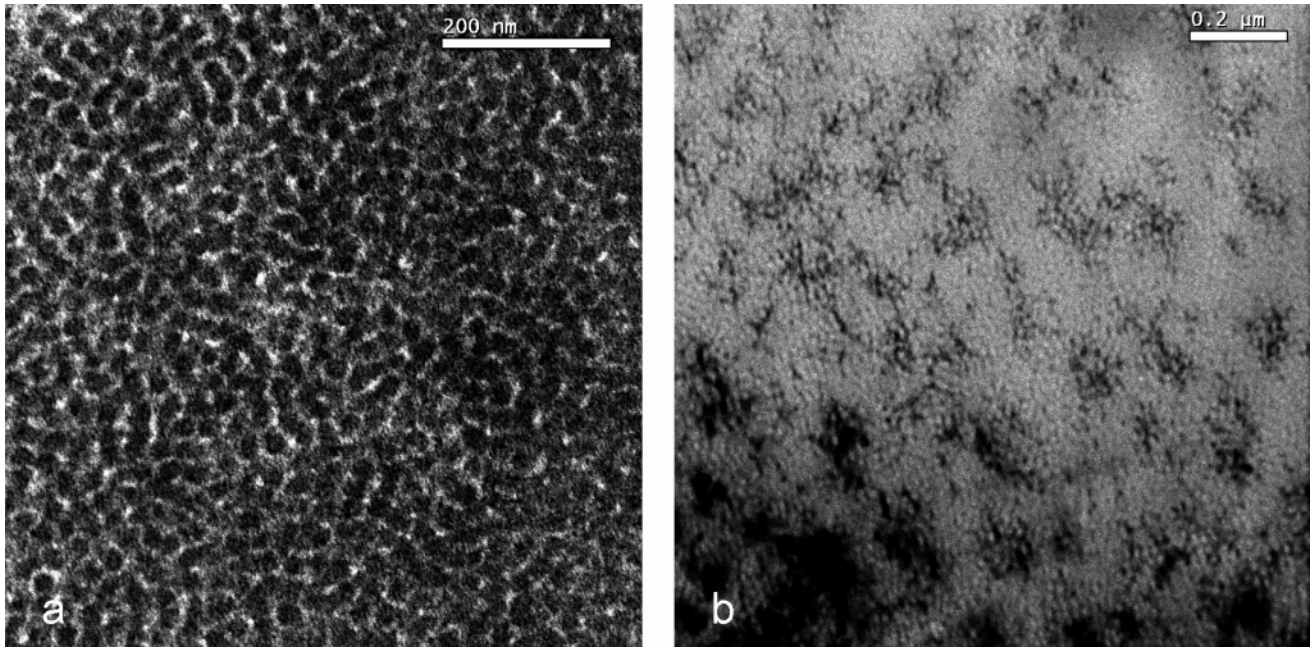

Figure 12. TEM pictures of polymers **6** (M_{150}:N_{50}) (a) and **9** (M_{50}:N_{150}) (b).

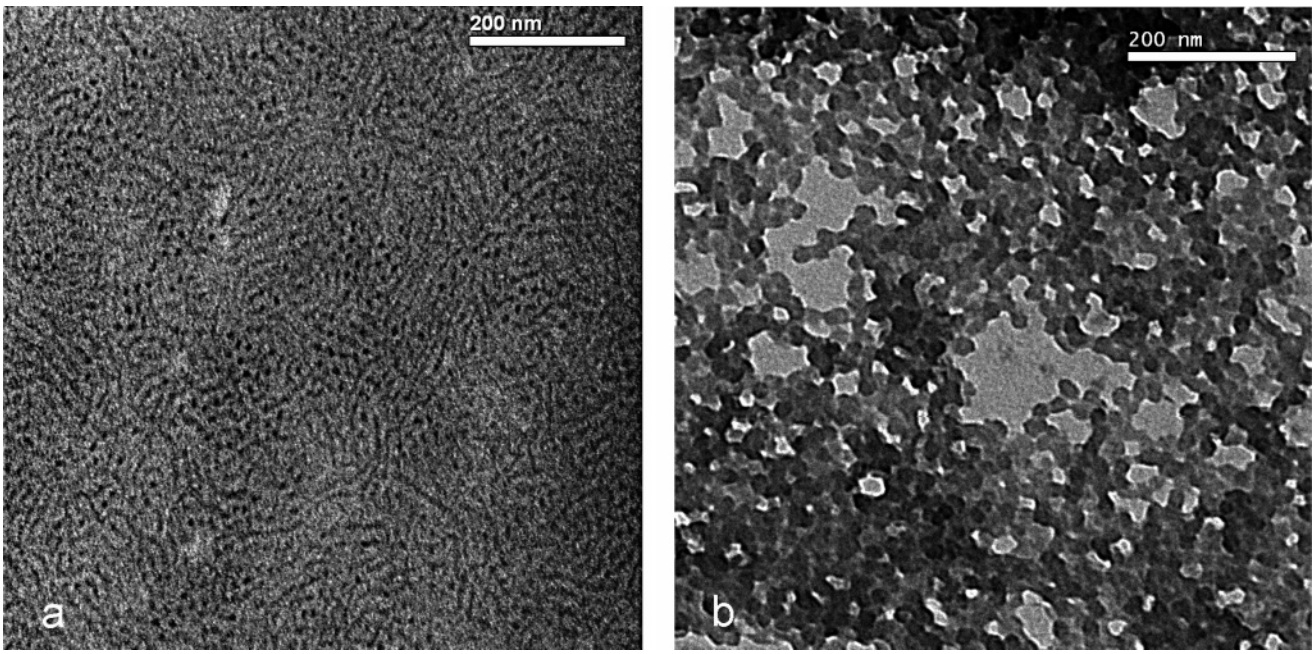

Figure 13. TEM image of polymers **5** (M_{175}:N_{25})and **10** (M_{25}:N_{175}).

low thermal stability of the carboxylic acid block that leads to anhydride formation upon heating does not allow the observation of thermal equilibrium phases for this type of polymer. However, we succeeded in preparing homogeneous polymer films by drop-casting from THF solutions which leads to a variety of different ordered morphologies. The SAXS and TEM investigations of the polymers **1**, **2**, **3**, and **7** with block ratios of 1:1 exhibit well self-organized lamellar phases. Polymer **8** exhibits an ordered hexagonal packed cylindrical phase. A liquidlike morphology with globular structures was found for polymer **6** (M_{150}:N_{50}) and **9** (M_{50}:N_{150}). Polymers **5** (M_{175}:N_{25})and **10** (M_{25}:N_{175}) show the less ordered structures. Polymer **5** shows well-separated small areas of the hydrophilic component embedded in the hydrophobic part, whereas polymer **10** shows globular connected structures of low order in the TEM images. This study on the self-assembly behavior of series of block copolymers shows that ROMP is a versatile method for the preparation of well-defined block copolymers. By tuning the composition of the block copolymer, a variety of different morphologies can be obtained. The potential of side- and end-functionalization as well as of the preparation of multiblock copolymers opens way to new highly ordered functionalized materials by ROMP.

Acknowledgment. Financial support by the Austrian Science Fund in the framework of the Austrian Nano-Initiative (Research Project Cluster 0700—Integrated Organic Sensor and Optoelectronics Technologies—Research Project Nos. 0701, 0705, and 0706) is gratefully acknowledged. The authors thank Christian Slugovc for helpful discussions, Petra Kaschnitz for the NMR measurements, and Josefine Hobisch for the GPC measurements.

Supporting Information Available: Explanation and citations about real-space interpretation of SAXS data. This material is available free of charge via the Internet at http://pubs.acs.org.

References and Notes

(1) Forster, S.; Plantenberg, T. *Angew. Chem., Int. Ed.* **2002**, *41*, 689−714.
(2) Lodge, T. P. *Macromol. Chem. Phys.* **2003**, *204*, 265−273.
(3) Castelletto, V.; Hamley, I. W. *Curr. Opin. Solid State Mater. Sci.* **2004**, *8*, 426−438.
(4) Matsen, M. W.; Bates, F. S. *Macromolecules* **1996**, *29*, 1091−1098.
(5) Hadjichristidis, N.; Pispas, S.; Floudas, G. A. *Block Copolymers−Synthetic Strategies, Physical Properties, and Applications;* John Wiley & Sons: Hoboken, NJ, 2003.
(6) Abetz, V.; Simon, P. F. W. *Adv. Polym. Sci.* **2005**, *189*, 125−212.
(7) Hong, K. L.; Uhrig, D.; Mays, J. W. *Curr. Opin. Solid State Mater. Sci.* **1999**, *4*, 531−538.
(8) Gan, L. H.; Ravi, P.; Mao, B. W.; Tam, K. C. *J. Polym. Sci., Part A: Polym. Chem.* **2003**, *41*, 2688−2695.
(9) Arotcarena, M.; Heise, B.; Ishaya, S.; Laschewsky, A. *J. Am. Chem. Soc.* **2002**, *124*, 3787−3793.
(10) Schrock, R. R. *Acc. Chem. Res.* **1990**, *23*, 158−165.
(11) Nguyen, S. T.; Johnson, L. K.; Grubbs, R. H.; Ziller, J. W. *J. Am. Chem. Soc.* **1992**, *114*, 3974−3975.
(12) Buchmeiser, M. R. *Chem. Rev.* **2000**, *100*, 1565−1604.
(13) Riegler, S.; Slugovc, C.; Trimmel, G.; Stelzer, F. *Macromol. Symp.* **2004**, *217*, 231−246.
(14) Choi, T. L.; Grubbs, R. H. *Angew. Chem., Int. Ed.* **2003**, *42*, 1743−1746.
(15) Bertin, P. A.; Smith, D. D.; Nguyen, S. T. *Chem. Commun.* **2005**, 3793−3795.
(16) Carrillo, A.; Kane, R. S. *J. Polym. Sci., Part A: Polym. Chem.* **2004**, *42*, 3352−3359.
(17) Chemtob, A.; Heroguez, V.; Gnanou, Y. *Macromolecules* **2004**, *37*, 7619−7627.
(18) Stubenrauch, K.; Moitzi, C.; Fritz, G.; Glatter, O.; Trimmel, G.; Stelzer, F. *Macromolecules* **2006**, *39*, 5865−5874.
(19) Dalphond, J.; Bazzi, H. S.; Kahrim, K.; Sleiman, H. F. *Macromol. Chem. Phys.* **2002**, *203*, 1988−1994.
(20) Ahmed, S. R.; Bullock, S. E.; Cresce, A. V.; Kofinas, P. *Polymer* **2003**, *44*, 4943−4948.
(21) Chen, B. Z.; Sleiman, H. F. *Macromolecules* **2004**, *37*, 5866−5872.
(22) Gratt, J.; Cohen, R. E. *Macromolecules* **1997**, *30*, 3137−3140.
(23) Kane, R. S.; Cohen, R. E.; Silbey, R. *Chem. Mater.* **1996**, *8*, 1919−1924.
(24) Cummins, C. C.; Beachy, M. D.; Schrock, R. R.; Vale, M. G.; Sankaran, V.; Cohen, R. E. *Chem. Mater.* **1991**, *3*, 1153−1163.
(25) Cummins, C. C.; Schrock, R. R.; Cohen, R. E. *Chem. Mater.* **1992**, *4*, 27−30.
(26) Chan, Y. N. C.; Schrock, R. R.; Cohen, R. E. *J. Am. Chem. Soc.* **1992**, 114, 7295−7296.
(27) Chan, Y. N. C.; Schrock, R. R.; Cohen, R. E. *Chem. Mater.* **1992**, *4*, 24−27.
(28) Chan, Y. N. C.; Craig, G. S. W.; Schrock, R. R.; Cohen, R. E. *Chem. Mater.* **1992**, *4*, 885−894.
(29) Sankaran, V.; Cohen, R. E.; Cummins, C. C.; Schrock, R. R. *Macromolecules* **1991**, *24*, 6664−6669.
(30) Sankaran, V.; Cummins, C. C.; Schrock, R. R.; Cohen, R. E.; Silbey, R. J. *J. Am. Chem. Soc.* **1990**, *112*, 6858−6859.
(31) Sankaran, V.; Yue, J.; Cohen, R. E.; Schrock, R. R.; Silbey, R. J. *Chem. Mater.* **1993**, *5*, 1133−1142.
(32) Yue, J.; Sankaran, V.; Cohen, R. E.; Schrock, R. R. *J. Am. Chem. Soc.* **1993**, *115*, 4409−4410.
(33) Ahmed, S. R.; Ogale, S. B.; Papaefthymiou, G. C.; Ramesh, R.; Kofinas, P. *Appl. Phys. Lett.* **2002**, *80*, 1616−1618.
(34) Clay, R. T.; Cohen, R. E. *Supramol. Sci.* **1997**, *2*, 183−191.
(35) Tassoni, R.; Schrock, R. R. *Chem. Mater.* **1994**, *6*, 744−749.
(36) Fogg, D. E.; Radzilowski, L. H.; Dabbousi, B. O.; Schrock, R. R.; Thomas, E. L.; Bawendi, M. G. *Macromolecules* **1997**, *30*, 8433−8439.
(37) Sohn, B. H.; Cohen, R. E. *J. Appl. Polym. Sci.* **1997**, *65*, 723−729.
(38) Saunders, R. S.; Cohen, R. E.; Schrock, R. R. *Macromolecules* **1991**, *24*, 5599−5605.
(39) Hamley, I. W.; Castelletto, V. *Prog. Polym. Sci.* **2004**, *29*, 909−948.
(40) Gottlieb, H. E.; Kotlyar, V.; Nudelman, A. *J. Org. Chem.* **1997**, *62*, 7512−7515.
(41) Schnablegger, H.; Glatter, O. *Appl. Opt.* **1991**, *30*, 4889−4896.
(42) Porod, G. *Kolloid Z. Z. Polym.* **1951**, *124*, 83−114.
(43) Vonk, C. G.; Kortleve, G. *Kolloid Z. Z. Polym.* **1967**, *220*, 19−24.
(44) Fourier, J. B. J. *Nouv. Bull. Sci. Soc. Philomatique Paris* **1808**, *1*, 112−116.
(45) Glatter, O. *J. Appl. Crystallogr.* **1980**, *13*, 577−584.
(46) Reinhold, C.; Fischer, E. W.; Peterlin, A. *J. Appl. Phys.* **1964**, *35*, 71−74.
(47) Glatter, O. *J. Appl. Crystallogr.* **1977**, *10*, 415−421.
(48) Glatter, O. *Acta Phys. Austriaca* **1977**, *47*, 83−102.
(49) Glatter, O. *J. Appl. Crystallogr.* **1979**, *12*, 166−175.
(50) BrunnerPopela, J.; Glatter, O. *J. Appl. Crystallogr.* **1997**, *30*, 431−442.
(51) Fritz, G.; Glatter, O. *J. Phys.: Condens. Matter* **2006**, *18*, S2403−S2419.
(52) Zernike, F.; Prins, J. A. *Z. Phys.* **1927**, *41*, 184−194.
(53) Barker, J. A.; Henderson, D. *J. Chem. Phys.* **1967**, *47*, 4714−4721.
(54) Percus, J. K.; Yevick, G. J. *Phys. Rev.* **1958**, *110*, 1−13.
(55) Ornstein, L. S. Z. F. *Koninklijke Akad. Wetenschappen/Afdeling Natuur* **1914**, 793−806.
(56) Socrates G, *Infrared Characteristic Group Frequencies*, 2nd ed.; Wiley: Chichester, 1994.
(57) Leibler, L. *Macromolecules* **1980**, *13*, 1602−1617.
(58) Fukunaga, K.; Elbs, H.; Magerle, R.; Krausch, G. *Macromolecules* **2000**, *33*, 947−953.
(59) Khandpur, A. K.; Forster, S.; Bates, F. S.; Hamley, I. W.; Ryan, A. J.; Bras, W.; Almdal, K.; Mortensen, K. *Macromolecules* **1995**, *28*, 8796−8806.
(60) Mani, S.; Weiss, R. A.; Hahn, S. F.; Williams, C. E.; Cantino, M. E.; Khairallah, L. H. *Polymer* **1998**, *39*, 2023−2033.
(61) Mittelbach, P.; Porod, G. *Acta Phys. Austriaca* **1961**, *14*, 405−439.
(62) Freiberger, N.; Moitzi, Ch.; de Campo, L.; Glatter, O. *J. Colloid Interface Sci.*, in press.

MA070181Q